

## Article

# Substitution of D-Arginine at Position 11 of $\alpha$ -RgIA Potently Inhibits $\alpha$ 7 Nicotinic Acetylcholine Receptor

Yong Wu <sup>1,\*</sup>, Junjie Zhang <sup>1</sup>, Jie Ren <sup>1</sup>, Xiaopeng Zhu <sup>1</sup>, Rui Li <sup>2</sup>, Dongting Zhangsun <sup>1,3</sup> and Sulan Luo <sup>1,3,\*</sup>

<sup>1</sup> School of Medicine, Guangxi University, Nanning 530004, China; zjjstudy@163.com (J.Z.); hndx2303@163.com (J.R.); zhuxiaopeng@gxu.edu.cn (X.Z.); zhangsundt@163.com (D.Z.)

<sup>2</sup> Shanghai Institute of Materia Medica, Chinese Academy of Sciences, Shanghai 201203, China; flychckn@163.com

<sup>3</sup> Key Laboratory of Tropical Biological Resources of Ministry of Education, Hainan University, Haikou 570228, China

\* Correspondence: wuyong@gxu.edu.cn (Y.W.); sulan2021@gxu.edu.cn (S.L.)

**Abstract:** Conotoxins are a class of disulfide-rich peptides found in the venom of cone snails, which have attracted considerable attention in recent years due to their potent activity on ion channels and potential for therapeutics. Among them,  $\alpha$ -conotoxin RgIA, a 13-residue peptide, has shown great promise as a potent inhibitor of  $\alpha$ 9 $\alpha$ 10 nAChRs for pain management. In this study, we investigated the effect of substituting the naturally occurring L-type arginine at position 11 of the RgIA sequence with its D-type amino acid. Our results indicate that this substitution abrogated the ability of RgIA to block  $\alpha$ 9 $\alpha$ 10 nAChRs, but instead endowed the peptide with the ability to block  $\alpha$ 7 nAChR activity. Structural analyses revealed that this substitution induced significant alteration of the secondary structure of RgIA[11r], which consequently affected its activity. Our findings underscore the potential of D-type amino acid substitution as a promising strategy for designing novel conotoxin-based ligands targeting different types of nAChRs.

**Keywords:** conotoxin; peptide synthesis; CD structure; electrophysiology; nicotinic acetylcholine receptors



**Citation:** Wu, Y.; Zhang, J.; Ren, J.; Zhu, X.; Li, R.; Zhangsun, D.; Luo, S. Substitution of D-Arginine at Position 11 of  $\alpha$ -RgIA Potently Inhibits  $\alpha$ 7 Nicotinic Acetylcholine Receptor. *Mar. Drugs* **2023**, *21*, 326. <https://doi.org/10.3390/md21060326>

Academic Editor: Sebastien Dutertre

Received: 15 April 2023

Revised: 23 May 2023

Accepted: 24 May 2023

Published: 26 May 2023



**Copyright:** © 2023 by the authors. Licensee MDPI, Basel, Switzerland. This article is an open access article distributed under the terms and conditions of the Creative Commons Attribution (CC BY) license (<https://creativecommons.org/licenses/by/4.0/>).

## 1. Introduction

Nicotinic acetylcholine receptors (nAChRs) are members of the Cys-loop ligand-gated ion channel superfamily which play crucial roles in rapid synaptic transmission and have been implicated in a range of nervous system diseases. To date, sixteen nAChR subunits ( $\alpha$ 1– $\alpha$ 7,  $\alpha$ 9,  $\alpha$ 10,  $\beta$ 1– $\beta$ 4,  $\gamma$ ,  $\delta$  and  $\epsilon$ ) have been identified in mammalian species. These subunits combine into hetero- or homo-pentamers to form nAChRs with different pharmacological and kinetic properties, as well as their localization [1]. The homomeric  $\alpha$ 7 nAChR has been intensely studied since its original discovery [2]. In the central nervous system,  $\alpha$ 7 nAChR is mainly distributed in the hippocampus and the cerebral cortex, regions associated with learning and memory mechanisms. Major human pathologies such as epilepsy, myasthenic syndromes, schizophrenia, Parkinson's and Alzheimer's diseases result from a dysfunction of  $\alpha$ 7 nAChR. Moreover,  $\alpha$ 7 nAChR is also located on the surface of macrophages, which plays a vital role in the cholinergic anti-inflammatory pathway. Therefore, ligands specifically designed to target the  $\alpha$ 7 receptor have the potential to be developed as drugs for the treatment of these diseases [3].

Conotoxins are a class of disulfide-rich peptides that are present in the venom of cone snails. Conotoxins have been shown to selectively and effectively modulate the function of ion channels and receptors in the nervous system [4]. Some of these peptides have been utilized as pharmacological probes, while others have been developed as potential drug leads. Notably,  $\omega$ -conotoxin MVIIA, which is known as Ziconotide or Prialt, is a well-known example of a conotoxin-derived drug that targets the calcium channel  $CaV_{2.2}$  and is

approved for the treatment of neuropathic pain [5,6]. Among the families of conotoxins,  $\alpha$ -conotoxins are distinguished by their selective antagonism against different subtypes of nAChRs, rendering them a significant source for the development of nAChR ligands. The  $\alpha$ -conotoxin family consists of peptides comprising 12–19 amino acids, which typically possess an amidated C-terminus, wherein the hydroxyl group of the carboxyl group is replaced with an amide. These peptides contain four cysteines (CysI-CysIII, CysII-CysIV), forming two pairs of disulfide bonds. Based on the number of amino acids between the cysteines (m/n), they can be categorized into various subtypes. In general, 3/5 (m/n)  $\alpha$ -conotoxins act as selective antagonists of muscle type, whereas 4/7, 4/4 and 4/3  $\alpha$ -conotoxins selectively antagonize non-muscle type nAChRs. The pharmacological effects of these peptides have been extensively investigated. Studies have demonstrated that the first loop harbors a conserved hydrophobic region, which determines its binding, whereas the second loop comprises a more variable region that confers selectivity. In vivo and in vitro, some of these peptides display therapeutic potential. Notably, some conotoxins have been found to inhibit the  $\alpha 7$  receptor with high affinity [4,7–9].

$\alpha$ -RgIA was discovered through cDNA sequencing of the venom gland of *Conus regius* [10]. The sequence and structure of this peptide are depicted in Figure 1. It belongs to the relatively uncommon class of  $\alpha 4/3$ -conotoxins, featuring four cysteines that form two pairs of disulfide bonds in the sequence and a high abundance of arginine residues. RgIA and its derivatives selectively and potently inhibit heterologous  $\alpha 9\alpha 10$  nAChR, which was found to be a neuropathic pain target. RgIA4, an analogue of RgIA, has garnered attention due to its high affinity towards human  $\alpha 9\alpha 10$  nAChRs [11]. The University of Utah has licensed RgIA4 to Kineta, under the designation KCP-400, for preclinical development [12]. However, the high arginine content of RgIA has raised concerns regarding its stability and in vivo bioavailability. To address this issue, we have employed a strategy of substituting amino acids with their D-form counterparts, leading to improved stability of RgIA while preserving its biological activity [13]. In this study, we have identified that one of the mutants containing a D-type amino acid substitution, RgIA[11r] (Figure 1), effectively inhibits the  $\alpha 7$  nAChR and significantly decreases the potency at the  $\alpha 9\alpha 10$  nAChR. These results suggest that D-type amino acid substitution not only enhances the stability of conotoxins but also enables the design of peptide ligands that can target other nAChR subtypes.

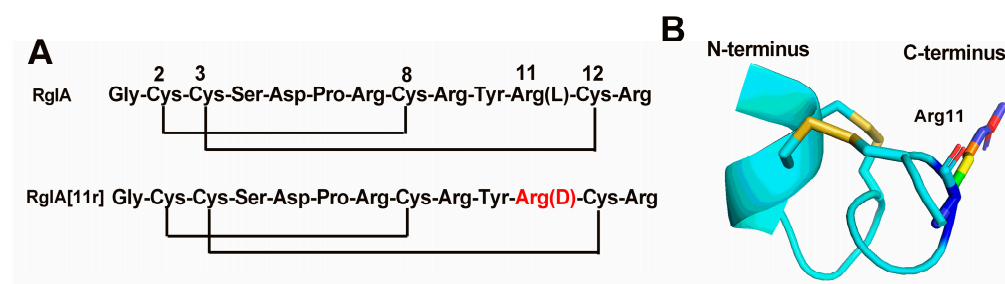


**Figure 1.** Sequences of conotoxins RgIA and RgIA[11r] and the three-dimensional structure of RgIA. (A) Amino acid sequences of RgIA and RgIA[11r] with two disulfide bonds. (B) The structure of RgIA arises from its interaction with the extracellular domain of the  $\alpha 9$  nAChR subunit (PDB: 6HY7) [14].

## 2. Results

### 2.1. Synthesis of RgIA and RgIA[11r]

This study employed the Fmoc solid-phase synthesis method to synthesize linear peptides of RgIA and RgIA[11r]. To produce RgIA[11r], the L-Arg residue at position 11 was substituted with D-Arg, yielding two peptides with identical theoretical molecular weights. To synthesize the folded peptides, a directed two-step folding approach was utilized. The Cys pairs were orthogonally protected using S-trityl (S-Trt) and acid-stable S-acetamidomethyl (S-Acm) groups. Selective removal of the S-trityl groups was achieved through cleavage from the resin, allowing the deprotected Cys residues to be oxidized with

20 mM potassium ferricyanide and 0.1 M Tris-HCl. Semi-preparative reversed phase-high-performance liquid chromatography (RP-HPLC) purification of the monocyclic peptide was then carried out, followed by treatment with iodine, resulting in the formation of the second disulfide bond between Cys3-Cys12. The molecular mass and purities of all peptides were validated with electrospray ionization–mass spectrometry (ESI-MS) and analytical RP-UPLC, respectively, as illustrated in Figure 2. The retention time of RgIA was 1.798 min, whereas that of RgIA[11r] was 1.717 min, indicating that RgIA[11r] was more hydrophilic when position 11 was substituted with D-Arg. The molecular weight of RgIA was determined to be 1571.13 Da, and that of RgIA[11r] was 1570.92 Da, consistent with the theoretical molecular weight. Our study demonstrates the successful synthesis and purification of folded RgIA and RgIA[11r] peptides using a directed two-step folding approach.

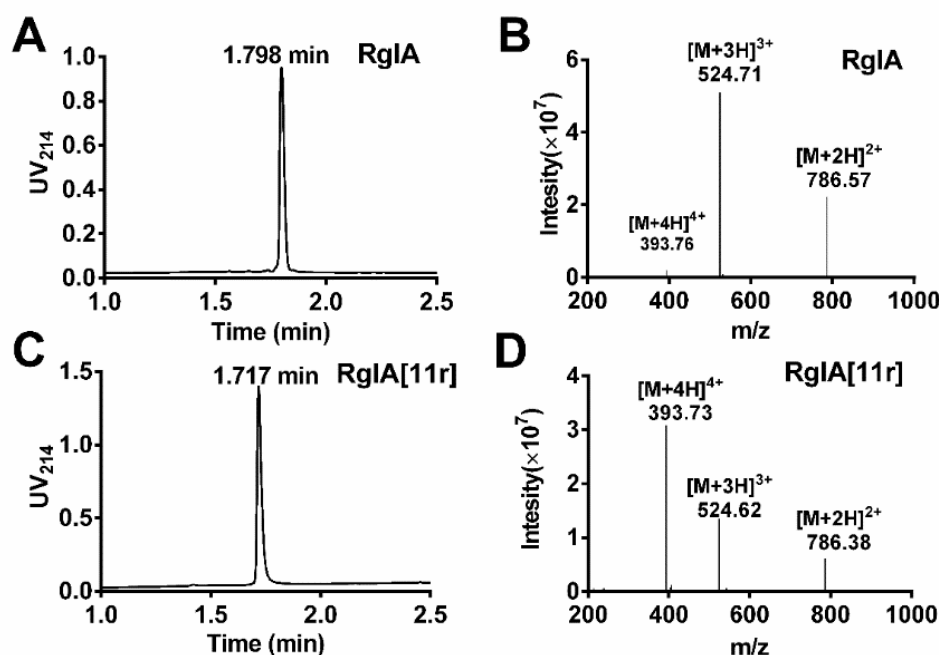


**Figure 2.** Analytical RP-UPLC profiles and ESI-MS spectra of  $\alpha$ -CTxs RgIA and RgIA[11r]. (A) RP-UPLC chromatogram of RgIA; (B) Electrospray ionization mass spectrometry (ESI-MS) data for RgIA with the observed monoisotopic mass of 1571.13 Da; (C) RP-UPLC chromatogram of RgIA[11r]; (D) ESI-MS data for RgIA[11r] with an observed monoisotopic mass of 1570.92 Da.

## 2.2. Potency of RgIA and RgIA[11r] at the Different Types of nAChRs

We conducted a comprehensive assessment of RgIA[11r]'s inhibitory activity (10  $\mu$ M) against various types of nAChRs, namely rat (r)  $\alpha$ 3 $\beta$ 2,  $\alpha$ 4 $\beta$ 4,  $\alpha$ 3 $\beta$ 4,  $\alpha$ 6/ $\alpha$ 3 $\beta$ 4,  $\alpha$ 4 $\beta$ 2,  $\alpha$ 2 $\beta$ 4,  $\alpha$ 7 and  $\alpha$ 9 $\alpha$ 10; and mouse (m)  $\alpha$ 1 $\beta$ 1 $\delta$  $\gamma$ , heterologously expressed in *Xenopus laevis* oocytes, using the two-electrode voltage clamp recording method. The results are presented in Figure 3. At  $\alpha$ 7 nAChRs, wild-type RgIA (10  $\mu$ M) demonstrated a 60% inhibitory effect on acetylcholine (ACh)-evoked currents. In contrast, RgIA[11r] displayed potent activity at  $\alpha$ 7 receptors, inhibiting approximately 95% of the ACh currents. Inhibition of other receptors was below 50% (Figure 3C). Remarkably, previous studies have reported that RgIA inhibits  $\alpha$ 9 $\alpha$ 10 at nanomolar levels [13]. However, surprisingly, 10  $\mu$ M RgIA[11r] only inhibited 60% of  $\alpha$ 9 $\alpha$ 10 ACh currents.

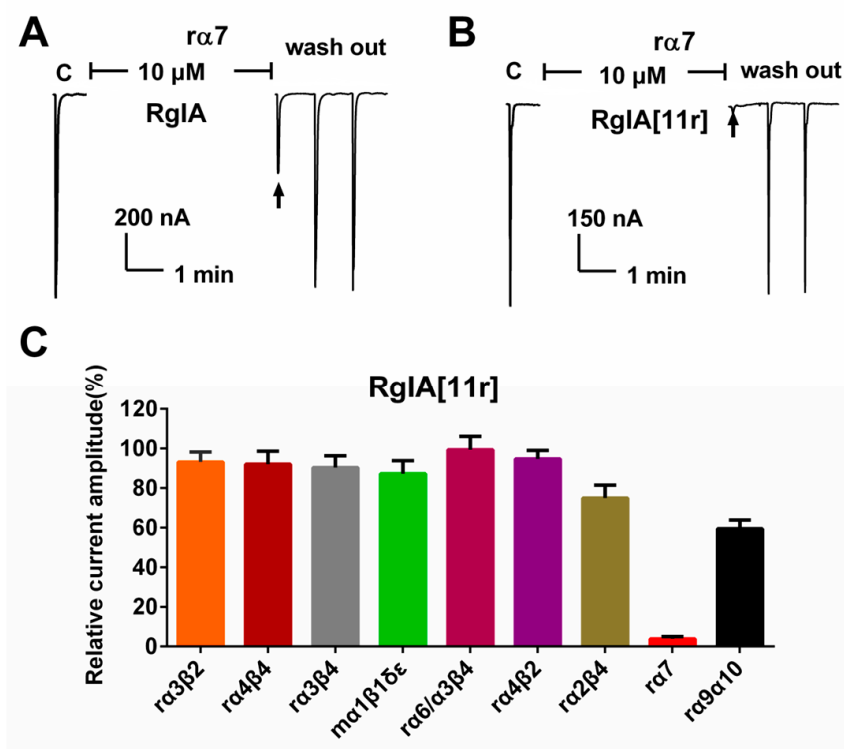


**Figure 3.** Inhibitory activity of RgIA and RgIA[11r] at different types of nAChRs. (A) Representative traces of ACh-evoked currents mediated by  $\alpha 7$  nAChRs in the presence of 10  $\mu\text{M}$  RgIA. (B) Representative traces of ACh-evoked currents mediated by  $\alpha 7$  nAChRs in the presence of 10  $\mu\text{M}$  RgIA[11r]. (C) Bar graph showing the inhibition of ACh-evoked peak current amplitude mediated by  $\alpha 3\beta 2$ ,  $\alpha 4\beta 4$ ,  $\alpha 3\beta 4$ ,  $\alpha 1\beta 1\delta\gamma$ ,  $\alpha 6/\alpha 3\beta 4$ ,  $\alpha 4\beta 2$ ,  $\alpha 2\beta 4$ ,  $\alpha 7$  and  $\alpha 9\alpha 10$  nAChRs by RgIA[11r] (10  $\mu\text{M}$ ). Data points represent mean  $\pm$  SEM ( $n = 3\text{--}6$ ).

The effective inhibition of  $\alpha 7$  nAChRs by RgIA at 10  $\mu\text{M}$  having been established, we proceeded to determine the concentration response relationships of RgIA and RgIA[11r] at  $\alpha 7$  and  $\alpha 9\alpha 10$  nAChRs (Figure 4). The corresponding half-maximal inhibitory concentration ( $\text{IC}_{50}$ ) values for their inhibition of ACh-evoked currents mediated by rat  $\alpha 7$  and  $\alpha 9\alpha 10$  nAChRs are summarized in Table 1. Wild-type RgIA displayed a robust antagonistic activity against  $\alpha 9\alpha 10$  receptors, exhibiting an  $\text{IC}_{50}$  value of 2.6 nM, but a weak activity against  $\alpha 7$ , with an  $\text{IC}_{50}$  of only 5313 nM, a result similar to those obtained previously [10]. In the present study, the replacement of the L-type arginine at position 11 with D-arginine resulted in the reversal of the activity of the mutant RgIA[11r]. RgIA[11r] showed inhibitory activity against  $\alpha 7$  with an  $\text{IC}_{50}$  of 163 nM, while it exhibited relatively minimal ( $\text{IC}_{50} = 15,820$  nM) against  $\alpha 9\alpha 10$ . Consequently, we proceeded to determine the inhibitory activity of RgIA and RgIA[11r] against human  $\alpha 9\alpha 10$  and  $\alpha 7$ , and the results are presented in Figure 4 and Table 1. Wild-type RgIA displayed weak activity against both human-derived  $\alpha 9\alpha 10$  and  $\alpha 7$  receptors, exhibiting  $\text{IC}_{50}$  values of 1398 and 4608 nM, respectively. Surprisingly, RgIA[11r] showed no detectable activity against  $\alpha 9\alpha 10$ , but still maintained a potency of 463 nM against  $\alpha 7$ . Overall, compared to the wild-type RgIA, RgIA[11r] demonstrated a significant enhancement in activity towards rat and human  $\alpha 7$  nAChRs, with an increase of 32.6-fold and 9.96-fold, respectively. However, its activity towards  $\alpha 9\alpha 10$  nAChRs was nearly completely lost. These findings suggest that the conformation of the arginine residue at position 11 of RgIA was altered, with significant effects on its inhibition at  $\alpha 7$  and  $\alpha 9\alpha 10$  nAChRs.

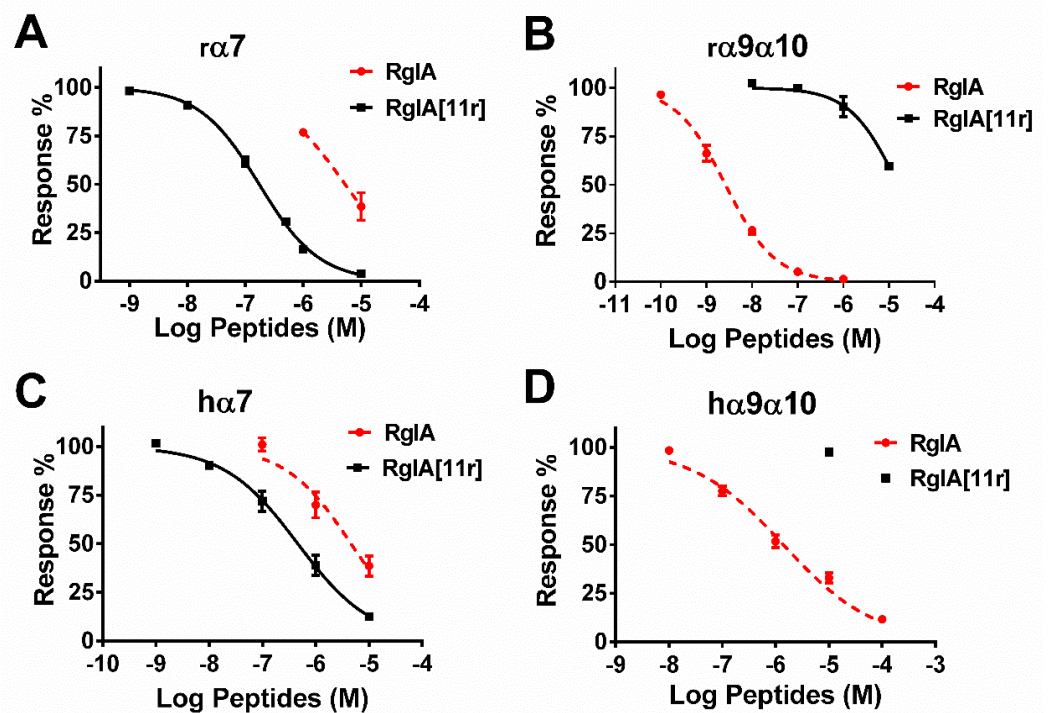


**Figure 4.** Concentration–response curves for the relative amplitude of ACh-evoked currents by RgIA and RgIA[11r] at different types of nAChRs; (A) rat  $\alpha 7$ , (B) rat  $\alpha 9\alpha 10$ , (C) human  $\alpha 7$  and (D) human  $\alpha 9\alpha 10$ . Data are presented as mean  $\pm$  SEM from 3 to 11 independent oocyte experiments.

**Table 1.** Inhibition of rat and human  $\alpha 7$  and  $\alpha 9\alpha 10$  nAChRs by RgIA and RgIA[11r].

Receptors	RgIA			RgIA[11r]			IC <sub>50</sub> Ratio of RgIA/RgIA[11r]
	IC <sub>50</sub> (95% CI *) (nM)	Hill Slope	<i>n</i>	IC <sub>50</sub> (95% CI *) (nM)	Hill Slope	<i>n</i>	
r $\alpha 7$	5313 (3068–9202)	0.8 (0.4–1.1)	3	163 (143–187)	0.8 (0.7–0.9)	11	32.6
h $\alpha 7$	4608 (2516–8440)	0.7 (0.4–1.0)	4	463 (333–640)	0.6 (0.5–0.7)	7	9.96
r $\alpha 9\alpha 10$	2.6 (2.1–3.2)	0.8 (0.7–0.9)	11	15,820 (10,380–24,200)	0.8 (0.5–1.2)	6	0.00016
h $\alpha 9\alpha 10$	1398 (997–1961)	0.5 (0.4–0.6)	6	>10,000	-	3	-

\* IC<sub>50</sub> values with 95% confidence interval; Hill slope obtained from the concentration–response curves for RgIA and RgIA[11r] at  $\alpha 7$  nAChRs. All data represent mean  $\pm$  SEM of *n* = 3–11 experiments.

### 2.3. Circular Dichroism (CD) Spectra of RgIA and RgIA[11r]

In this study, we compared the secondary structure conformation of RgIA with that of RgIA[11r] using CD spectroscopic analysis (Figure 5). The 3D structure of RgIA is shown in Figure 1B, with a type I  $\beta$ -turn at its N-terminus from Cys2 to Asp5, while loop II from Tyr10–Cys12 is less well-defined. Our results show that when L-Arg residue at position 11 was replaced with a D-Arg residue, its negative absorption peak at 208 nm and its positive absorption peak at 222 nm were enhanced. This suggests that there may be a tendency for the formation of  $\alpha$ -helix at Loop II of RgIA[11r], which indicates that the structure of RgIA is altered when the arginine of 11 is replaced by D-type amino acid. This result is significantly different from our previous study, where the replacement of Arg-13 by D-Arg had less effect on the structure of RgIA [13].

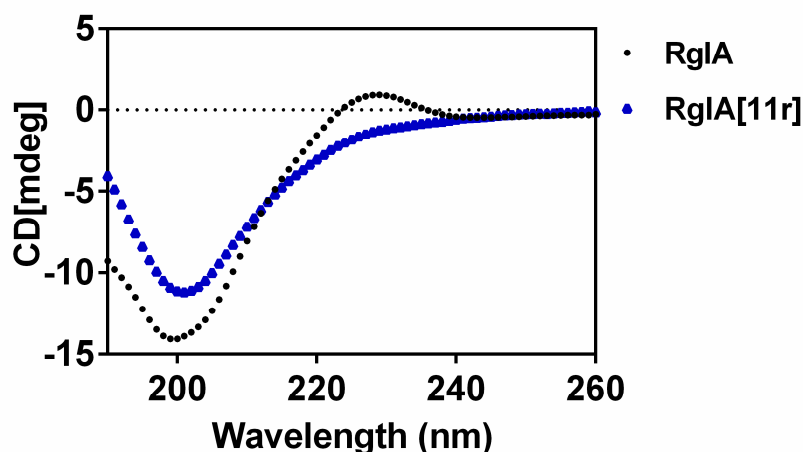


Figure 5. Circular dichroism spectra of RgIA and RgIA[11r].

#### 2.4. Serum Stability of RgIA and RgIA[11r]

We assessed the stability of wild-type RgIA and its 11-position D-amino acid substitution mutant, RgIA[11r], in human serum. The experimental results, as depicted in Figure 6, indicated poor stability for both peptides, with complete degradation observed within 30 min. This suggests that the substitution of individual amino acids with D-amino acids did not significantly enhance peptide stability. Our previous research has demonstrated a notable improvement in stability when all arginine residues were replaced with D-amino acids [13].

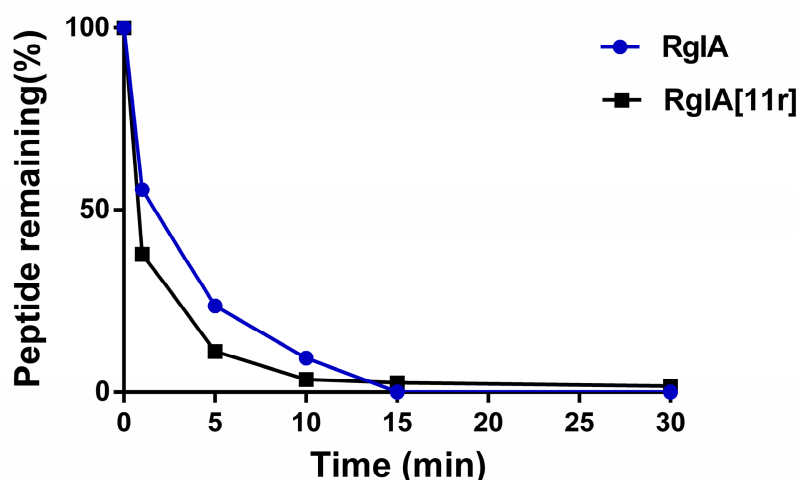
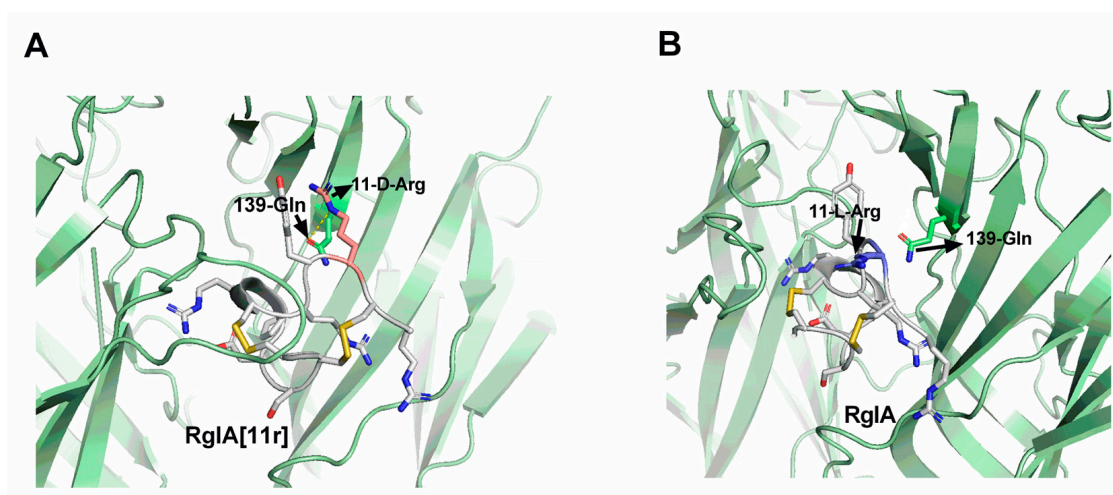


Figure 6. Serum stability of RgIA and RgIA[11r]. Error bars represent the mean  $\pm$  SEM ( $n = 6$ ).

#### 2.5. Molecular Docking (MD) Demonstrates Altered Potency between RgIA[11r] and $\alpha 7$ nAChRs

To further analyze the molecular mechanism underlying the targeting of the  $\alpha 7$  nAChRs by RgIA[11r], we performed separate molecular docking studies between RgIA and RgIA[11r] with the human  $\alpha 7$  nAChRs. The docking results, as illustrated in Figure 7, revealed that the 11-position D-amino acid in RgIA[11r] formed a hydrogen bond with residue 139-Gln in the extracellular region of the  $\alpha 7$  nAChRs, while RgIA itself did not exhibit any interactions with the  $\alpha 7$  nAChRs. The docking scores indicated a value of  $-10.8$  kcal/mol for RgIA[11r] and  $-9.9$  kcal/mol for RgIA when docked with the  $\alpha 7$  nAChRs, suggesting an increased ligand affinity following the D-amino acid substitution mutation.



**Figure 7.** Molecular docking of RgIA/RgIA[11r] with  $h\alpha 7$  nAChRs. **(A)** Molecular docking of RgIA[11r] with  $h\alpha 7$  nAChRs, demonstrating the formation of hydrogen bonds between 11-D-Arg and the neighboring residue 139-Gln of the  $\alpha 7$  nAChR. **(B)** Molecular docking of RgIA with  $h\alpha 7$  nAChR, indicating the absence of interactions between 11-L-Arg and other residues of the  $\alpha 7$  nAChR. The images were generated using PyMOL.

### 3. Discussion

Initially, we used D-alanine scanning to study the key amino acid residues of RgIA and found that, except for arginine at position 13, the activity was greatly reduced after replacing the amino acids at other positions with D-amino acids [13]. Based on the synthesized D-type RgIA derivatives, we tested the activity of other subtypes of nAChRs and were surprised to find that RgIA[11r] had strong inhibition activity against the  $\alpha 7$  nAChRs. Building on this finding, we discovered that RgIA[11r] had strong blocking activity against human and murine  $\alpha 7$  nAChRs.

Previous research has indicated that homomeric  $\alpha 7$  nAChRs play a significant role in regulating neuropsychiatric and neurological disorders, as well as the inflammatory response of immune cells [15,16]. Given their potential as targets for treating inflammatory and neuropathic pain, the crucial physiological functions of  $\alpha 7$  nAChRs have sparked considerable interest in developing drugs that target these receptors. Agonists or antagonists of  $\alpha 7$  have emerged as promising candidates for drug development to treat  $\alpha 7$ -related diseases [2]. Numerous  $\alpha$ -conotoxins and their analogues that can inhibit  $\alpha 7$  nAChRs have been discovered (Table 2). Among these,  $\alpha 4/3$ -conotoxins ImI and ImII have been extensively studied and found to block various nAChR subtypes. In the case of  $\alpha 7$  nAChRs, different research groups have reported varying potencies [17,18]. Multiple  $\alpha 4/7$ -conotoxins, such as GID, OmIA and PeIA, inhibiting  $\alpha 7$  nAChRs with high potency, have demonstrated blocking effects on different types of nAChRs, with particularly strong activity against  $\alpha 3\beta 2$  nAChRs. The ArIB mutant ArIB [V11L, V16A] has potent activity targeting  $\alpha 7$  nAChRs, with  $IC_{50}$ s as low as picomolar levels, and a certain inhibitory effect at  $\alpha 6/\alpha 3\beta 2\beta 3$  nAChRs. In our laboratory, the  $\alpha 4/4$ -conotoxin [Q1G, $\Delta$ R14]LvIB had strong activity at rat  $\alpha 7$  nAChRs, but low activity against human receptors [19]. In this study, RgIA[11r] exhibited an  $IC_{50}$  of 463 nM and 163 nM at human and rat  $\alpha 7$  nAChRs, respectively. In comparison to other  $\alpha$ -conotoxins acting on  $\alpha 7$  nAChRs, RgIA[11r], although not the most potent, displayed relatively good selectivity for the  $\alpha 7$  subtype with negligible inhibition at other nAChR subtypes. It is known that certain conotoxin peptides exhibit high activity against murine receptors but weak activity against human receptors, thereby limiting their clinical potential. The present investigation demonstrated that RgIA[11r] also exhibited higher activity against  $h\alpha 7$  nAChRs, and therefore holds significant medicinal value. It is plausible that this peptide may serve as a framework for designing more potent peptide ligands targeting  $h\alpha 7$  nAChRs.

**Table 2.** Inhibition of  $\alpha 7$  nAChRs by  $\alpha$ - conotoxins.

Name	Sequences	$\alpha 7$ (IC <sub>50</sub> , nM)	Other nAChR Subtypes	Ref.
RgIA[11r]	GCCSDPRCRYrCR	r $\alpha 7$ (163) > h $\alpha 7$ (463)	>10,000	This work
RegIIA	GCCSHPACNVNPNPHIC #	r $\alpha 7$ (41) > h $\alpha 7$ (210)	$\alpha 3\beta 2 > \alpha 3\beta 4 > \alpha 7$ $\alpha 6 / \alpha 3\beta 4\beta 3$	[20,21]
[H5D]RegIIA	GCCSDPACNVNPNPHIC #	r $\alpha 7$ (100) > h $\alpha 7$ (13,680)	N.D.	[20]
OmIA	GCCSHPACNVNPNPHICG #	r $\alpha 7$ (59) > h $\alpha 7$ (290)	$\alpha 3\beta 2 > \alpha 6 / \alpha 3\beta 2 > \alpha 7$	[22]
PnIA	GCCSLPPCAANNPD(sTy)C #	h $\alpha 7$ -5HT3 chimaera (510), r $\alpha 7$ (252)	$\alpha 3\beta 2 > \alpha 7$	[23,24]
PnIA [A10L,sTy15Y]	GCCSLPPCALNNPDYC #	r $\alpha 7$ (12) > h $\alpha 7$ (59)	$\alpha 3\beta 2 \approx \alpha 7$	[20]
[Q1G, $\Delta$ R14]LvIB	GCCSNPPCAHEHC #	r $\alpha 7$ (97) > h $\alpha 7$ (1570)	$\alpha 7 > \alpha 6 / \alpha 3\beta 2\beta 3 > r\alpha 3\beta 2 > r\alpha 6 / \alpha 3\beta 4$	[19]
ImI	GCCSDPRCAWRC #	r $\alpha 7$ (69) > h $\alpha 7$ (440)	h $\alpha 3\beta 2 \approx \alpha 7$	[17,18]
ImII	ACCSDPACAWRC #	r $\alpha 7$ (441) > h $\alpha 7$ (571)	$\alpha 7 > \alpha 1\beta 1\delta\epsilon$	[17]
LsIA	SGCCSNPACRVNPNPHIC #	h $\alpha 7$ (10.1)	$\alpha 7 \approx \alpha 3\beta 2 > \alpha 3\alpha 5\beta 2$	[25]
ArIA	IRDECCSNPACRVNPNPHVCRRR	r $\alpha 7$ (6.02)	$\alpha 7 > \alpha 3\beta 2$	[24]
ArIB	DECCSNPACRVNPNPHVCRRR	r $\alpha 7$ (1.81)	$\alpha 7 > \alpha 6 / \alpha 3\beta 2\beta 3 > \alpha 3\beta 2$	[24]
ArIB [V11L, V16A]	DECCSNPACRLNPNPHVCRRR	r $\alpha 7$ (0.356)	$\alpha 7 > \alpha 6 / \alpha 3\beta 2\beta 3 > \alpha 3\beta 2$	[24]
EpI	GCCSDPRCNMNNPD(sTy)C #	r $\alpha 7$ (30)	$\alpha 7 > \alpha 3\beta 4$	[26,27]
GID	IRD(Gla)CCSNPACRVNNOHVC	h $\alpha 7$ (4.5) > r $\alpha 7$ (5.1)	$\alpha 3\beta 2 > \alpha 7 > \alpha 3\beta 4$	[28,29]

sTy refers to sulphytyrosine; O is hydroxyproline; Gla is  $\gamma$ -carboxyglutamic acid; # denotes C-terminal carboxamide.

Amino acids exist as two enantiomers: L and D, except for glycine, which lacks a chiral center. Although the D-amino acid (D-AA) enantiomer of  $\alpha$ -amino acids was once considered unimportant in biological systems, it has garnered significant interest among researchers due to its ability to improve protein stability. One of the major challenges in peptide development is their susceptibility to degradation by proteases, resulting in a short half-life in the human intestine, plasma and cells. Therefore, enhancing peptide stability and bioavailability is crucial to improve their medicinal value. To address this challenge, analogues such as cyclodextrin (D)-amino-acid-engineered analogues have been designed to prolong their half-life in humans [30]. It is well recognized that the conversion of one enantiomer to another in a biological system can cause significant structural changes in peptides or proteins, which can affect their function and biological activity. The inversion of stereochemistry at the chiral center and the corresponding conformational preferences of D-AAAs to their L-counterparts often lead to instability of the secondary structure when D-AAAs are incorporated into L-peptides or proteins. However, it has been observed that peptides with  $\alpha$ -helix, long  $\beta$ -strand and long loop structures are generally less sensitive to substitution with D-AAAs than short  $\beta$ -strands [31]. In this study, we observed changes in the structure when arginine at the 11th position was replaced with the D-form, as determined by CD spectra. Although the amino acid sequence of conotoxin peptides is short, their spatial structure is compact, and the amino acids located in the loop formed by cysteine residues have a significant impact on their activity and selectivity. In the present investigation, the substitution of the 11th arginine residue with a D-configured amino acid resulted in the loss of the peptide's original activity and a shift towards antagonizing  $\alpha 7$  nAChRs. We utilized molecular docking to elucidate the molecular mechanism of interaction between the mutant RgIA[11r] and h $\alpha 7$  nAChRs. Our findings reveal the formation of new hydrogen bonds. However, our previous studies have demonstrated that when other residues except for Arg-11 in RgIA were substituted with D-configuration, no activity towards h $\alpha 7$  nAChRs was observed [13]. This suggests that the substitution of peptides with D-configured amino acids requires careful consideration and further investigation. Nevertheless, this study provides a direction for the subsequent design highly selective and active conotoxins.

## 4. Materials and Methods

### 4.1. Materials

Clones of rat ( $\alpha$ 2,  $\alpha$ 3,  $\alpha$ 4,  $\alpha$ 7 and  $\beta$ 2,  $\beta$ 3 and  $\beta$ 4, as well as mouse (m)  $\alpha$ 1,  $\beta$ 1,  $\delta$  and  $\epsilon$  cDNAs were generously provided by S. Heinemann (Salk Institute, La Jolla, CA, USA). It is worth noting that the  $\alpha$ 6 subunit is difficult to express in vitro, so we constructed the  $\alpha$ 6/ $\alpha$ 3 chimeric subunit instead, which consisted of the N-terminal extracellular ligand-binding domain of the  $\alpha$ 6 subunit and the remainder as the  $\alpha$ 3 subunit segment. The  $\alpha$ 6/ $\alpha$ 3 chimera clone was generously provided by J. E. Garrett (Cognetix, Inc., Salt Lake City, UT, USA). Clones of  $\alpha$ 9 and  $\alpha$ 10 were kindly provided by A.B. Elgoyen (Instituto de Investigaciones en Ingeniería Genética y Biología Molecular, Buenos Aires, Argentina). C. W. Luetje (University of Miami, Miami, FL, USA) provided clones of  $\beta$ 2 and  $\beta$ 3 subunits in the high-expressing pGEMHE vector. The RNAs of human  $\alpha$ 7,  $\alpha$ 9 and  $\alpha$ 10 nAChRs were synthesized using mMessage mMachine transcription kit (Ambion, Foster City, CA, USA). The mMESSAGING mMACHINE in vitro Transcription Kit and an RNA MEGA Clear Kit were purchased from Thermo Fisher Scientific (Austin, TX, USA). Acetylcholine chloride, atropine and bovine serum albumin (BSA) were obtained from Sigma (St. Louis, MO, USA). Acetonitrile (ACN, HPLC grade) was purchased from Thermo Fisher Scientific (Pittsburgh, PA, USA). Trifluoroacetic acid (TFA) was purchased from Tedia Company (Fairfield, OH, USA). Vitamin C (VC),  $K_3[Fe(CN)_6]$ ,  $I_2$  and other reagents were purchased from Guangzhou Chemical Reagent Company (Guangzhou, China). All standard amino acids, and preloaded resin for peptide synthesis, were purchased from GL Biochem (Shanghai, China). Side-chain protection for the following amino acids was as follows: L-Arg and D-Arg, 2,2,4,6,7-pentamethyl-dihydrobenzofuran-5-sulfonyl (Pbf); Ser, Tyr, tert-butyl (tBu); Cys, acetamidomethyl (Acm) and Cys, trityl (Trt). All other chemicals were analytical-grade and were obtained from Sigma. Reverse-phase (RP) HPLC analytical Symmetry Shield RP18 column (5  $\mu$ m, 4.6  $\times$  150 mm, 130-Å pore size), RP-UPLC ACQUITY UPLC BEH C18 column (1.7  $\mu$ m, 2.1  $\times$  50 mm, 130-Å pore size) and preparative XBridge Peptide BEH C18 column (5  $\mu$ m, 19  $\times$  100 mm, 130-Å pore size) were obtained from Waters Corp. (Milford, MA, USA). The female *Xenopus laevis* used for experiments were obtained from Nasco (Fort Atkinson, WI, USA) and were housed at 17 °C in our laboratory animal room and fed twice a week. All animal experiments were conducted in accordance with ethical standards for animal research (GXU-2023-0060).

### 4.2. RgIA and RgIA[11r] Synthesis

The synthesis of conopeptides was accomplished on a 0.05 mmol scale using a Liberty Blue automated peptide synthesizer (CEM, Charlotte, NC, USA), applying standard solid-phase Fmoc (9-fluorenylmethyloxycarbonyl) protocols using Fmoc-Arg(Pbf) Wang resin (0.49 mmol/g load). During the assembly process, Cys3 and Cys12 were integrated into the peptide chain with Acm side chain protection to aid in regioselective disulfide formation, while Cys2 and Cys8 were protected with Trt side chain. The peptides were subsequently cleaved from the resin with trifluoroacetic acid (TFA) in the presence of tri-isopropylsilane (TIPS) and water (9:0.5:0.5 (v/v/v) TFA:TIPS:water) at room temperature for 2 h, resulting in simultaneously removing the side-chain-protecting groups, except for cysteines with Acm. Then, the cleavage mixture was filtered and precipitated with 40 mL of cold ether. The crude peptide was then precipitated by centrifugation at 9000  $\times$  g for 15 min and washed twice with approximately 40 mL of cold ether, air-dried and then dissolved in 5 mL 0.05% TFA, 50% acetonitrile containing and vacuum lyophilized. The crude peptides were solubilized with 50 mL of HPLC buffer B, diluted to 10-fold volume prior to purification by Semi-preparative RP-HPLC, using a preparative XBridge Peptide BEH C18 column eluted with a linear gradient ranging from 2 to 50% buffer B in 48 min at a flow rate 12 mL/min. The buffers were 0.05% (v/v) TFA in water (buffer A) and 0.05% TFA (v/v) in 60% aqueous acetonitrile (v/v) (buffer B). The eluent was monitored by measuring absorbance at 214 nm. The purity of the peptide was assessed by ACQUITY UPLC BEH C18 column RP-HPLC (buffer A: 0.05% (v/v) TFA in water; buffer B: 90% aqueous acetonitrile (v/v)) using the

same gradient as described above with a flow rate 0.5 mL/min. The peptide solution with higher purity was collected, put into a  $-80\text{ }^{\circ}\text{C}$  ultra-low temperature refrigerator overnight, and then frozen into powder by vacuum freeze-dryer. The linear peptides were then dissolved in 0.1 M Tris-HCl buffer containing 20 mM potassium ferricyanide to facilitate the formation of the first disulfide. The second disulfide bond was formed through iodine oxidation, as previously described [32]. The purity of RgIA and RgIA[11r] was confirmed using analytical RP-UPLC as described for the linear peptide after oxidative folding. Finally, electrospray mass spectrometry was utilized to confirm the molecular weight of the synthetic peptides. The purity for all fully folded peptides was  $\geq 95\%$  and was determined using analytical RP-UPLC.

#### 4.3. cRNA Preparation and Injection into *Xenopus laevis* Oocytes

The plasmids containing the human, rat and mouse nAChR subunits were linearized using an appropriate restriction enzyme (TaKaRa, Kyoto, Japan). Capped RNA was synthesized in vitro for these subunits using the T7 mMessage mMachine Transcription Kit (Ambion, Austin, TX, USA) and purified using the MEGA clear<sup>TM</sup> Transcription clean-up Kit (Invitrogen; Thermo Fisher Scientific, Inc., Austin, TX, USA). The concentration of each cRNA was determined at 260 nm using a Smart Spec<sup>TM</sup> plus Spectrophotometer (Bio-Rad, Hercules, CA, USA). To produce 200–500 ng/ $\mu\text{L}$  of cRNA for each subunit, the various subunit cRNAs were mixed with ratio 1:1, and 50 nL aliquots were injected into the cytoplasm of the oocytes using a Drummond microdispenser (Drummond Scientific, Broomall, PA, USA). The oocytes were then incubated at  $18\text{ }^{\circ}\text{C}$  in ND-96 buffer (96 mM NaCl, 2 mM KCl, 1.8 mM  $\text{CaCl}_2$ , 1 mM  $\text{MgCl}_2$  and 5 mM HEPES, pH 7.4) containing 10 mg/L penicillin, 10 mg/L streptomycin and 100 mg/L gentamicin.

#### 4.4. Electrophysiological Recordings

As previously reported [33], *Xenopus* oocytes were analyzed using the two-electrode voltage-clamp method 3–5 days after injection. The oocytes were recorded using an Axoclamp 900A amplifier (Molecular Devices Corp., Sunnyvale, CA, USA) and the Clampfit 10.2 software (Molecular Devices Corp., Sunnyvale, CA, USA). The oocyte chamber was a cylindrical groove with a volume of approximately 50  $\mu\text{L}$ , which was perfused with ND-96 buffer containing 0.1 mg/mL BSA at a flow rate of 2–4 mL/min under gravity. During the recording, the oocytes were held at a voltage of  $-70\text{ mV}$  and stimulated with a one-second pulse of 200  $\mu\text{M}$  ACh every minute to stimulate  $\alpha 7$  nAChRs. After establishing a stable baseline, the flow of buffer was stopped, and the oocytes were pre-incubated for 5 min with pure ND-96 or ND-96 containing different concentrations of conotoxins before the recovery of the ACh pulse.

#### 4.5. Statistical Analysis

The percentage of response to conotoxin was obtained by dividing the toxin response by the pre-intoxication baseline value. Dose–response data were analyzed using GraphPad Prism 6.0 software (GraphPad Software, San Diego, CA, USA) and fitted with the formula: percentage response =  $100 / (1 + ([\text{toxin}] / \text{IC}_{50})^{\text{nH}})$ , where nH is the Hill coefficient. Each data point on the dose–response curve represents the mean  $\pm$  S.E. of at least three oocytes. The  $\text{IC}_{50}$  values with 95% confidence interval were determined by nonlinear regression analysis with GraphPad Prism software.

#### 4.6. Circular Dichroism (CD) Spectroscopy

CD spectra of RgIA and RgIA[11r] in aqueous solution were obtained using a Chirascan CD spectrometer (Applied Photophysics, Leatherhead, UK). The CD spectra were recorded at room temperature under a constant nitrogen flush. The peptides were dissolved in water at a concentration of 200  $\mu\text{M}$  and measurements were performed in a 1 mm quartz cuvette. Peptide spectral data were recorded in the far UV range (190–260 nm) with a step size and bandwidth of 1 nm. The spectra were obtained from the average of five measure-

ments after subtraction of the background signal, which was also averaged. The spectra were expressed in units of molar ellipticity ( $\theta$ ) using Applied Photophysics Chirascan and Photophysics Chirascan software (Applied Photophysics, Leatherhead, U.K.).

#### 4.7. Serum Stability Assay

Serum stability assays were conducted employing human serum sourced from male AB plasma (Sigma-Aldrich, Darmstadt, Germany) following a modified protocol as previously described by Andrew et al. [34]. Human serum was subjected to an additional incubation period of 15 min at 37 °C prior to the commencement of the assay. Triplicate samples of peptides were dissolved in Milli-Q water at a concentration of 1 mg/mL and subsequently diluted with serum to a concentration of 0.1 mg/mL. The samples were then incubated at 37 °C, and 20  $\mu$ L aliquots were collected at specific time intervals of 0, 1, 5, 10, 15, 30, 60, 120, 240 and 480 min. Each sample underwent denaturation by adding an equal volume of 6 M urea and incubating at 4 °C for 10 min. Following denaturation, precipitation was achieved by adding an equal volume of 20% trichloroacetic acid at 4 °C for 10 min. The samples were subsequently centrifuged at 14,000 rpm for 10 min, and 10  $\mu$ L of the resulting supernatant was analyzed using RP-UPLC. Each sample was subjected to repeated analysis twice. The remaining percentage of the peptide was determined by comparing the areas under the curve to the samples measured at the initial time point (0 min).

#### 4.8. Docking

The glide docking method was employed to construct the ligand–receptor complex. As a template, the cocrystal structure of RgIA and RgIA[11r] in complex with the  $\alpha$ 7 (PDB: 7EKT) was utilized. The three-dimensional structures of RgIA were retrieved from the RCSB database (PDB: 2JUT). Subsequently, the native RgIA was subjected to RgIA[11r] using Schrödinger software (2020, New York, USA). The dimensions of the simulation box were set as ligand of template. The docking procedure utilized the standard precision (SP) method for docking precision and employed a flexible ligand sampling approach. Specifically, 50 poses per ligand were generated. To assess the binding affinity of each ligand, the docking score calculation was employed to determine the potency of each pose [35,36].

### 5. Conclusions

In this study, the D-type amino acid RgIA[11r] mutant of RgIA lost its inhibitory activity at the  $\alpha$ 9 $\alpha$ 10 nAChRs, but gained the ability to selectively target and inhibit both human and rat  $\alpha$ 7 nAChRs, while not inhibiting other subtypes of nAChRs. The pharmacological profile of RgIA[11r] renders it a promising molecular probe for studying  $\alpha$ 7 nAChRs, and it also demonstrates the potential for therapeutic applications. In addition, the findings from this study suggest that D-type amino acid substitution can modify not only peptide stability, but also peptide activity. Therefore, it represents an effective strategy for peptide modification, and has the potential to lead to the discovery of novel peptide-based therapeutics with improved properties.

**Author Contributions:** Conceptualization and Methodology: Y.W. and S.L.; Writing—original draft preparation: Y.W.; Writing—Review and Editing: Y.W., X.Z. and S.L.; Experiment: J.R., Y.W., R.L. and J.Z.; Supervision: S.L. and D.Z. All authors have read and agreed to the published version of the manuscript.

**Funding:** These studies were supported by the National Natural Science Foundation of China (No. 32170534), Guangxi Science and Technology Base and Talent Special Project (2021AC19001), Guangxi Science and Technology Base & Talents Fund (GUIKE AD22035948), Major Intergovernmental Joint Research Project of National Key R & D Program of China (2022YFE0132700) and the 111 Project (D20010), Innovation Project of Guangxi Graduate Education (YCSW2022072).

**Institutional Review Board Statement:** Not applicable.

**Informed Consent Statement:** Not applicable.

**Data Availability Statement:** The data presented in this study are available in the article.

**Conflicts of Interest:** The authors declare no competing financial interest.

## References

1. Albuquerque, E.X.; Pereira, E.F.; Alkondon, M.; Rogers, S.W. Mammalian nicotinic acetylcholine receptors: From structure to function. *Physiol. Rev.* **2009**, *89*, 73–120. [[CrossRef](#)] [[PubMed](#)]
2. Hone, A.J.; McIntosh, J.M. Nicotinic acetylcholine receptors: Therapeutic targets for novel ligands to treat pain and inflammation. *Pharmacol. Res.* **2023**, *190*, 106715. [[CrossRef](#)] [[PubMed](#)]
3. Ramos-Martinez, I.E.; Rodriguez, M.C.; Cerbon, M.; Ramos-Martinez, J.C.; Ramos-Martinez, E.G. Role of the Cholinergic Anti-Inflammatory Reflex in Central Nervous System Diseases. *Int. J. Mol. Sci.* **2021**, *22*, 13427. [[CrossRef](#)]
4. Akondi, K.B.; Muttenthaler, M.; Dutertre, S.; Kaas, Q.; Craik, D.J.; Lewis, R.J.; Alewood, P.F. Discovery, synthesis, and structure-activity relationships of conotoxins. *Chem. Rev.* **2014**, *114*, 5815–5847. [[CrossRef](#)]
5. Patel, R.; Montagut-Bordas, C.; Dickenson, A.H. Calcium channel modulation as a target in chronic pain control. *Br. J. Pharmacol.* **2018**, *175*, 2173–2184. [[CrossRef](#)]
6. Molinski, T.F.; Dalisay, D.S.; Lievens, S.L.; Saludes, J.P. Drug development from marine natural products. *Nat. Rev. Drug Discov.* **2009**, *8*, 69–85. [[CrossRef](#)]
7. Vetter, I.; Lewis, R.J. Therapeutic potential of cone snail venom peptides (conopeptides). *Curr. Top. Med. Chem.* **2012**, *12*, 1546–1552. [[CrossRef](#)]
8. Jin, A.H.; Muttenthaler, M.; Dutertre, S.; Himaya, S.W.A.; Kaas, Q.; Craik, D.J.; Lewis, R.J.; Alewood, P.F. Conotoxins: Chemistry and Biology. *Chem. Rev.* **2019**, *119*, 11510–11549. [[CrossRef](#)]
9. Halai, R.; Craik, D.J. Conotoxins: Natural product drug leads. *Nat. Prod. Rep.* **2009**, *26*, 526–536. [[CrossRef](#)]
10. Ellison, M.; Haberlandt, C.; Gomez-Casati, M.E.; Watkins, M.; Elgoyhen, A.B.; McIntosh, J.M.; Olivera, B.M.  $\alpha$ -RgIA: A novel conotoxin that specifically and potently blocks the  $\alpha$ 9 $\alpha$ 10 nAChR. *Biochemistry* **2006**, *45*, 1511–1517. [[CrossRef](#)]
11. Romero, H.K.; Christensen, S.B.; Di Cesare Mannelli, L.; Gajewiak, J.; Ramachandra, R.; Elmslie, K.S.; Vetter, D.E.; Ghelardini, C.; Iadonato, S.P.; Mercado, J.L.; et al. Inhibition of  $\alpha$ 9 $\alpha$ 10 nicotinic acetylcholine receptors prevents chemotherapy-induced neuropathic pain. *Proc. Natl. Acad. Sci. USA* **2017**, *114*, E1825–E1832. [[CrossRef](#)]
12. Safavi-Hemami, H.; Brogan, S.E.; Olivera, B.M. Pain therapeutics from cone snail venoms: From Ziconotide to novel non-opioid pathways. *J. Proteomics* **2019**, *190*, 12–20. [[CrossRef](#)] [[PubMed](#)]
13. Ren, J.; Zhu, X.; Xu, P.; Li, R.; Fu, Y.; Dong, S.; Zhangsun, D.; Wu, Y.; Luo, S. D-Amino Acid Substitution of  $\alpha$ -Conotoxin RgIA Identifies its Critical Residues and Improves the Enzymatic Stability. *Mar. Drugs* **2019**, *17*, 142. [[CrossRef](#)] [[PubMed](#)]
14. Zouridakis, M.; Papakyriakou, A.; Ivanov, I.A.; Kasheverov, I.E.; Tsetlin, V.; Tzartos, S.; Giastas, P. Crystal Structure of the Monomeric Extracellular Domain of  $\alpha$ 9 Nicotinic Receptor Subunit in Complex With  $\alpha$ -Conotoxin RgIA: Molecular Dynamics Insights Into RgIA Binding to  $\alpha$ 9 $\alpha$ 10 Nicotinic Receptors. *Front. Pharm.* **2019**, *10*, 474. [[CrossRef](#)]
15. Pavlov, V.A.; Wang, H.; Czura, C.J.; Friedman, S.G.; Tracey, K.J. The cholinergic anti-inflammatory pathway: A missing link in neuroimmunomodulation. *Mol. Med.* **2003**, *9*, 125–134. [[CrossRef](#)] [[PubMed](#)]
16. Baez-Pagan, C.A.; Delgado-Velez, M.; Lasalde-Dominicci, J.A. Activation of the Macrophage  $\alpha$ 7 Nicotinic Acetylcholine Receptor and Control of Inflammation. *J. Neuroimmune Pharmacol.* **2015**, *10*, 468–476. [[CrossRef](#)]
17. Ellison, M.; Gao, F.; Wang, H.L.; Sine, S.M.; McIntosh, J.M.; Olivera, B.M. A-conotoxins ImI and ImII target distinct regions of the human  $\alpha$ 7 nicotinic acetylcholine receptor and distinguish human nicotinic receptor subtypes. *Biochemistry* **2004**, *43*, 16019–16026. [[CrossRef](#)]
18. Armishaw, C.J.; Daly, N.L.; Nevin, S.T.; Adams, D.J.; Craik, D.J.; Alewood, P.F. A-selenoconotoxins, a new class of potent  $\alpha$ 7 neuronal nicotinic receptor antagonists. *J. Biol. Chem.* **2006**, *281*, 14136–14143. [[CrossRef](#)]
19. Wang, S.; Zhu, X.; Zhangsun, M.; Wu, Y.; Yu, J.; Harvey, P.J.; Kaas, Q.; Zhangsun, D.; Craik, D.J.; Luo, S. Engineered Conotoxin Differentially Blocks and Discriminates Rat and Human  $\alpha$ 7 Nicotinic Acetylcholine Receptors. *J. Med. Chem.* **2021**, *64*, 5620–5631. [[CrossRef](#)]
20. Yu, J.; Zhu, X.; Zhang, L.; Kudryavtsev, D.; Kasheverov, I.; Lei, Y.; Zhangsun, D.; Tsetlin, V.; Luo, S. Species specificity of rat and human  $\alpha$ 7 nicotinic acetylcholine receptors towards different classes of peptide and protein antagonists. *Neuropharmacology* **2018**, *139*, 226–237. [[CrossRef](#)]
21. Kompella, S.N.; Cuny, H.; Hung, A.; Adams, D.J. Molecular Basis for Differential Sensitivity of  $\alpha$ -Conotoxin RegIIA at Rat and Human Neuronal Nicotinic Acetylcholine Receptors. *Mol. Pharmacol.* **2015**, *88*, 993–1001. [[CrossRef](#)] [[PubMed](#)]
22. Talley, T.T.; Olivera, B.M.; Han, K.H.; Christensen, S.B.; Dowell, C.; Tsigelny, I.; Ho, K.Y.; Taylor, P.; McIntosh, J.M. A-conotoxin OmIA is a potent ligand for the acetylcholine-binding protein as well as  $\alpha$ 3 $\beta$ 2 and  $\alpha$ 7 nicotinic acetylcholine receptors. *J. Biol. Chem.* **2006**, *281*, 24678–24686. [[CrossRef](#)]
23. Armishaw, C.; Jensen, A.A.; Balle, T.; Clark, R.J.; Harpsoe, K.; Skonberg, C.; Liljefors, T.; Stromgaard, K. Rational design of  $\alpha$ -conotoxin analogues targeting  $\alpha$ 7 nicotinic acetylcholine receptors: Improved antagonistic activity by incorporation of proline derivatives. *J. Biol. Chem.* **2009**, *284*, 9498–9512. [[CrossRef](#)] [[PubMed](#)]

24. Whiteaker, P.; Christensen, S.; Yoshikami, D.; Dowell, C.; Watkins, M.; Gulyas, J.; Rivier, J.; Olivera, B.M.; McIntosh, J.M. Discovery, synthesis, and structure activity of a highly selective  $\alpha 7$  nicotinic acetylcholine receptor antagonist. *Biochemistry* **2007**, *46*, 6628–6638. [[CrossRef](#)] [[PubMed](#)]
25. Inserra, M.C.; Kompella, S.N.; Vetter, I.; Brust, A.; Daly, N.L.; Cuny, H.; Craik, D.J.; Alewood, P.F.; Adams, D.J.; Lewis, R.J. Isolation and characterization of  $\alpha$ -conotoxin LsIA with potent activity at nicotinic acetylcholine receptors. *Biochem. Pharmacol.* **2013**, *86*, 791–799. [[CrossRef](#)]
26. Nicke, A.; Samochocki, M.; Loughnan, M.L.; Bansal, P.S.; Maelicke, A.; Lewis, R.J. A-conotoxins EpI and AuIB switch subtype selectivity and activity in native versus recombinant nicotinic acetylcholine receptors. *FEBS Lett.* **2003**, *554*, 219–223. [[CrossRef](#)] [[PubMed](#)]
27. Ho, T.N.T.; Lee, H.S.; Swaminathan, S.; Goodwin, L.; Rai, N.; Ushay, B.; Lewis, R.J.; Rosengren, K.J.; Conibear, A.C. Posttranslational modifications of  $\alpha$ -conotoxins: Sulfotyrosine and C-terminal amidation stabilise structures and increase acetylcholine receptor binding. *RSC. Med. Chem.* **2021**, *12*, 1574–1584. [[CrossRef](#)]
28. Millard, E.L.; Nevin, S.T.; Loughnan, M.L.; Nicke, A.; Clark, R.J.; Alewood, P.F.; Lewis, R.J.; Adams, D.J.; Craik, D.J.; Daly, N.L. Inhibition of Neuronal Nicotinic Acetylcholine Receptor Subtypes by  $\alpha$ -Conotoxin GID and Analogues. *J. Biol. Chem.* **2009**, *284*, 4944–4951. [[CrossRef](#)]
29. Nicke, A.; Loughnan, M.L.; Millard, E.L.; Alewood, P.F.; Adams, D.J.; Daly, N.L.; Craik, D.J.; Lewis, R.J. Isolation, structure, and activity of GID, a novel  $\alpha$  4/7-conotoxin with an extended N-terminal sequence. *J. Biol. Chem.* **2003**, *278*, 3137–3144. [[CrossRef](#)]
30. Tugyi, R.; Uray, K.; Ivan, D.; Fellingner, E.; Perkins, A.; Hudecz, F. Partial D-amino acid substitution: Improved enzymatic stability and preserved Ab recognition of a MUC2 epitope peptide. *Proc. Natl. Acad. Sci. USA* **2005**, *102*, 413–418. [[CrossRef](#)]
31. Shen, J. D-Amino acid substituted peptides as potential alternatives of homochiral L-configurations. *Amino Acids* **2021**, *53*, 265–280. [[CrossRef](#)] [[PubMed](#)]
32. Luo, S.; Zhangsun, D.; Zhu, X.; Wu, Y.; Hu, Y.; Christensen, S.; Harvey, P.J.; Akcan, M.; Craik, D.J.; McIntosh, J.M. Characterization of a novel  $\alpha$ -conotoxin TxID from *Conus textile* that potently blocks rat  $\alpha 3\beta 4$  nicotinic acetylcholine receptors. *J. Med. Chem.* **2013**, *56*, 9655–9663. [[CrossRef](#)] [[PubMed](#)]
33. Luo, S.; Zhangsun, D.; Schroeder, C.I.; Zhu, X.; Hu, Y.; Wu, Y.; Weltzin, M.M.; Eberhard, S.; Kaas, Q.; Craik, D.J.; et al. A novel  $\alpha 4/7$ -conotoxin LvIA from *Conus lividus* that selectively blocks  $\alpha 3\beta 2$  vs.  $\alpha 6/\alpha 3\beta 2\beta 3$  nicotinic acetylcholine receptors. *FASEB J.* **2014**, *28*, 1842–1853. [[CrossRef](#)]
34. White, A.M.; de Veer, S.J.; Wu, G.; Harvey, P.J.; Yap, K.; King, G.J.; Swedberg, J.E.; Wang, C.K.; Law, R.H.P.; Durek, T.; et al. Application and structural analysis of triazole-bridged disulfide mimetics in cyclic peptides. *Angew. Chem.* **2020**, *59*, 11273–11277. [[CrossRef](#)] [[PubMed](#)]
35. Halgren, T.A.; Murphy, R.B.; Friesner, R.A.; Beard, H.S.; Frye, L.L.; Pollard, W.T.; Banks, J.L. Glide: A new approach for rapid, accurate docking and scoring. 2. Enrichment factors in database screening. *J. Med. Chem.* **2004**, *47*, 1750–1759. [[CrossRef](#)]
36. Friesner, R.A.; Banks, J.L.; Murphy, R.B.; Halgren, T.A.; Klicic, J.J.; Mainz, D.T.; Repasky, M.P.; Knoll, E.H.; Shelley, M.; Perry, J.K.; et al. Glide: A new approach for rapid, accurate docking and scoring. 1. Method and assessment of docking accuracy. *J. Med. Chem.* **2004**, *47*, 1739–1749. [[CrossRef](#)]

**Disclaimer/Publisher’s Note:** The statements, opinions and data contained in all publications are solely those of the individual author(s) and contributor(s) and not of MDPI and/or the editor(s). MDPI and/or the editor(s) disclaim responsibility for any injury to people or property resulting from any ideas, methods, instructions or products referred to in the content.